

Intrinsic superconducting diode effects in tilted Weyl and Dirac semimetalsKai Chen, Bishnu Karki , and Pavan Hosur*Department of Physics and Texas Center for Superconductivity, University of Houston, Houston, Texas 77204, USA* (Received 22 September 2023; revised 16 January 2024; accepted 30 January 2024; published 20 February 2024)

We explore Weyl and Dirac semimetals with tilted nodes as platforms for realizing an intrinsic superconducting diode effect. Although tilting breaks sufficient spatial and time-reversal symmetries, we prove that — at least for conventional *s*-wave singlet pairing — the effect is forbidden by an emergent particle-hole symmetry at low energies if the Fermi level is tuned to the nodes. Then, as a stepping stone to the three-dimensional semimetals, we analyze a minimal one-dimensional model with a tilted helical node using Ginzburg-Landau theory. While one might expect a drastic enhancement of the effect when the node turns from type-I to type-II, we find that the presence of multiple Fermi pockets is more important as it enables multiple pairing amplitudes with independent contributions to supercurrents in opposite directions. Equipped with this insight, we construct minimal lattice models of Weyl and Dirac semimetals and study the superconducting diode effect in them. Once again, we see an enhancement when the normal state has multiple Fermi pockets per node that can accommodate more than one pairing channel. In summary, this study sheds light on the key factors governing the intrinsic superconducting diode effect in systems with asymmetric band structures and paves the way for realizing it in topological semimetals.

DOI: [10.1103/PhysRevB.109.064511](https://doi.org/10.1103/PhysRevB.109.064511)**I. INTRODUCTION**

In recent years, there has been a growing interest in the field of electronics and superconductivity due to the fascinating observation of superconducting diode effects (SDEs). These effects involve the ability of certain materials and structures to exhibit nonreciprocal superconducting transport, effectively blocking electric current flow in one direction while allowing it to pass in the opposite direction. This behavior resembles that of a diode, making SDEs crucial for devising rectifiers and switches.

A seminal experimental study by Ando *et al.* [1] demonstrated the presence of SDEs in an artificial superlattice [Nb/V/Ta]. This observation was achieved by breaking the inversion symmetry of the structure and introducing time-reversal symmetry breaking through the application of an external magnetic field. Since then, the study of SDEs has become an active area of research in the field of superconductivity, owing to the significant potential of the nonreciprocal critical supercurrent in various applications, such as electronics, spintronics, phase-coherent charge transport, direction-selective charge transport, and quantum computation using superconductor qubits [2–7].

Experimental investigations have explored SDEs in diverse materials and structures. For instance, SDEs have been observed in magic angle twisted graphenes [8–10] and in few-layer NbSe₂ [11]. Furthermore, Josephson supercurrent diode effects have been demonstrated in highly transparent Josephson junctions fabricated on InAs quantum wells [12], in van der Waals heterostructures and symmetric Al/InAs-2DEG/Al junctions [13], in a three-terminal Josephson device based upon an InAs quantum well [14], and Josephson junctions containing single magnetic atoms [15]. The thin superconducting films made of niobium and

vanadium indicate a robust SDE when exposed to an extremely low magnetic field of 1 Oe. Furthermore, when a layer of EuS is introduced, the SDE is amplified [16]. For asymmetric vortex motion, which exposes the mechanism underpinning the superconducting vortex diode phenomenon, has been reported in the layered structure of Nb/EuS (superconductor/ferromagnet) [17]. SDE has also been observed in topological insulator/superconductor [18–20] and superconductor nanowire/topological Dirac semimetal [21] hybrid systems.

The intriguing experimental findings have stimulated theoretical efforts to understand the underlying mechanisms of SDEs. The Rashba-Zeeman-Hubbard model has been proposed as a theoretical framework to explain SDEs, and established a close relationship between SDE and Fulde-Ferrell-Larkin-Ovchinnikov (FFLO) states [22,23]. In the FFLO state, Cooper pairs form with finite center-of-mass momenta due to opposite spin states on Zeeman-split Fermi surfaces [24,25]. Numerical calculations and Ginzburg-Landau (GL) theory have provided further support and insights into the understanding of SDEs [23,26]. Among extrinsic mechanisms, SDE behavior has been predicted in topological insulators and Rashba nanowires [27] as well as general metallic wires with asymmetric dispersion, with the latter expected to show the theoretically maximum SDE in a range of parameters [28]. Moreover, researchers have investigated the influence of disorder on SDEs by using the quasiclassical Eilenberger equation [29]. The disorder effect is crucial in comprehending the behavior of SDEs in realistic and practical scenarios. Theoretical studies have also focused on the Josephson diode effect, revealing its universality and potential applicability in various contexts [27,30–33].

Recent experiments have drawn attention to superconductivity in topological semimetals, prompting substantial efforts

in the quest for topological superconductors among various materials. For example, in the Dirac material PdTe, its surface states show a fully gapped superconducting Cooper pairing structure below T_c , and its bulk hosts nodal gap structures due to spin-orbit coupling [34]. The type-II Dirac semimetal PdTe2 is an intrinsic superconductor below T_c with a conventional fully gapped order parameter [35–37]. In addition, intrinsic superconductivity is also observed in NbC [38] and in $\text{Ir}_{1-x}\text{Pt}_x\text{Te}_2$ [39]. Superconductivity can be induced via tips and pressure in type-I Weyl semimetal TaP [40,41]. It can also be induced through the application of hydrostatic pressure in the type-II Weyl semimetal MoTe2 and the three-dimensional Dirac semimetal Cd_3As_2 [42–45]. By conducting hard point contact measurements on nonsuperconducting topological semimetals using nonsuperconducting metallic tips can induce superconductivity in the contact region. This method is capable of enhancing the T_c for some superconductors, such as Au_2Pb [46]. Furthermore, the superconductivity in a transition-metal dipnictide like NbAs_2 can be induced by pressure, causing a structural phase transition [47].

In semimetals, lattice symmetries, interactions, and strong spin-orbit coupling can give rise to a rich variety of pairing states [48–50]. The nontrivial Berry curvature at the Fermi surface of Weyl semimetals leads to a pairing function with no specific momentum dependence, enabling the realization of topological superconductors [51]. Weyl semimetals can support effective s -wave and p -wave pair correlations through opposite pseudospin and equal pseudospin channels. By tuning the parameters, the effective s -wave and p -wave symmetry classes can evolve into d -wave and f -wave classes [52]. On the other hand, a magnetic Weyl semimetal sandwiched between two conventional s -wave spin-singlet superconductors can exhibit interorbital s -wave pairing, featuring both even-frequency spin-singlet and odd-frequency mixed-spin-triplet symmetry [53]. In this work, we explore intrinsic SDEs in semimetals, focusing on s -wave pairing for its simplicity and commonality in phonon-mediated superconductivity. Our aim is to illustrate SDEs arising from the band structure rather than pairing symmetry.

Weyl and Dirac semimetals are characterized by gapless points between their valence and conduction bands, known as Weyl and Dirac points, respectively [54–59]. They possess several favorable properties that make them promising platforms for the SDEs. For instance, the density of states near the nodes is low, which facilitates breaking of time-reversal, inversion and spatial symmetries necessary for enabling the SDE. These materials also typically have multiple Fermi pockets centered at different points in momentum space, which enhances the possibility of FFLO states [48–50,60]. Moreover, Fermi pockets centered around the origin can also develop finite momentum pairing if the dispersion is tilted. There are two different types of Weyl/Dirac semimetals: type I, with point-like Fermi surfaces, and type II, defined by electron and hole pockets touching at the Weyl nodes [61–63]. Tilting the dispersion around the node induces the transition from type-I to type-II. In this study, we shed light on the key factors that enhance the SDE in tilted semimetals. In particular, we show that multiple inequivalent pairing channels can enhance the intrinsic SDEs and are more important than the band tilting.

The outline of this paper is as follows. In Sec. II, we delve into the symmetries beyond time reversal and inversion symmetry that need to be broken to support SDEs. We explore how tuning the chemical potential impacts these symmetries, shedding light on the underlying symmetry breaking responsible for SDEs, and offering potential avenues for experimental control and manipulation of these effects. In Sec. III, we employ the Ginzburg-Landau theory to investigate a one-dimensional model characterized by an asymmetric band structure. Our analysis reveals that this simple yet insightful model can indeed support a ground state with Cooper pairs possessing finite momentum, thus providing a compelling platform to observe and study SDEs. Building on the insights gained from the one-dimensional (1D) model, we extend our study to lattice modes of tilted Weyl semimetals and Dirac semimetals in Secs. IV and V, respectively. Our numerical simulations reveal the existence of nonreciprocity in the depairing critical current, the key requirement for SDEs in these intriguing materials, and support the heuristic that multiple inequivalent pairing channels are more important than band asymmetry for a large SDE.

II. SYMMETRY AND THE ROLE OF CHEMICAL POTENTIAL μ

In general, the necessary conditions for realizing the SDE are the violation of time-reversal (\mathcal{T}), inversion (\mathcal{I}), and spatial symmetries under which current in the desired nonreciprocal direction is odd. These conditions ensure the breaking of reciprocity in the system, meaning that the response of the superconductor to external perturbations is different for the perturbations applied in opposite directions. In most cases, these violations suffice to guarantee a SDE; however, a chiral or particle hole symmetry in the normal state, common found at low energies near band intersections, can suppress the SDE for singlet pairing as shown below.

Consider a Bloch Hamiltonian $H(\mathbf{k})$. The Bogoliubov–de Gennes (BdG) Hamiltonian for generic pairing in the basis $(c_{\mathbf{k}+\mathbf{q}/2}, c_{-\mathbf{k}+\mathbf{q}/2}^\dagger)^T$ is

$$H^{\text{BdG}}(\mathbf{k}, \mathbf{q}, \Delta_{\mathbf{k}}) = \begin{pmatrix} H(\mathbf{k} + \mathbf{q}/2) & \Delta_{\mathbf{k}} \\ \Delta_{\mathbf{k}}^\dagger & -H^*(-\mathbf{k} + \mathbf{q}/2) \end{pmatrix}, \quad (1)$$

where we allow for pairing with finite momentum \mathbf{q} and fermion antisymmetry ensures $\Delta_{\mathbf{k}} = -\Delta_{-\mathbf{k}}^T$. $H^{\text{BdG}}(\mathbf{k}, \mathbf{q}, \Delta)$ obeys particle-hole symmetry

$$\tau_x \mathbb{K} H^{\text{BdG}}(\mathbf{k}, \mathbf{q}, \Delta_{\mathbf{k}}) \mathbb{K} \tau_x = -H^{\text{BdG}}(-\mathbf{k}, \mathbf{q}, \Delta_{\mathbf{k}}), \quad (2)$$

where τ_x is a Pauli matrix in Nambu space and \mathbb{K} denotes complex conjugation.

Suppose the normal state also has a chiral unitary symmetry Q :

$$QH(\mathbf{k})Q^\dagger = -H(\mathbf{k}), \quad (3)$$

or a chiral antiunitary or particle-hole symmetry $Q\mathbb{K}$:

$$Q\mathbb{K}H(\mathbf{k})\mathbb{K}Q^\dagger = -H^*(-\mathbf{k}). \quad (4)$$

Under Q and $Q\mathbb{K}$, $H^{\text{BdG}}(\mathbf{k}, \mathbf{q}, \Delta_{\mathbf{k}})$ transforms into $-H^{\text{BdG}}(\mathbf{k}, \mathbf{q}, -\tilde{\Delta}_{\mathbf{k}})$ and $-\tau_x H^{\text{BdG}}(-\mathbf{k}, \mathbf{q}, \tilde{\Delta}_{\mathbf{k}}) \tau_x$, respectively, where $\tilde{\Delta}_{\mathbf{k}} = Q\Delta_{\mathbf{k}}Q^\dagger$. Along with the BdG particle-hole

symmetry Eq. (2), these two symmetries in the normal state ensure that $H^{\text{BdG}}(\mathbf{k}, \mathbf{q}, \Delta_{\mathbf{k}})$ is related to $H^{\text{BdG}}(\mathbf{k}, -\mathbf{q}, -\Delta_{\mathbf{k}})$ and $H^{\text{BdG}}(-\mathbf{k}, -\mathbf{q}, \Delta_{\mathbf{k}})$ by antiunitary and unitary operations.

Assuming the electrons experience an attractive Hubbard interaction ($g > 0$)

$$H_{\text{int}} = -g \sum_{\mathbf{k}, \mathbf{k}', \mathbf{q}} c_{\mathbf{k}+\frac{\mathbf{q}}{2}\uparrow}^\dagger c_{-\mathbf{k}+\frac{\mathbf{q}}{2}\downarrow}^\dagger c_{-\mathbf{k}+\frac{\mathbf{q}}{2}\downarrow} c_{\mathbf{k}'+\frac{\mathbf{q}}{2}\uparrow}, \quad (5)$$

where g represents the strength of attraction. Within the mean-field approximation, we get the Ginzburg-Landau free energy density

$$f(\mathbf{q}, \Delta) = \int_{\mathbf{k}} \frac{\text{tr}(\Delta_{\mathbf{k}} \Delta_{\mathbf{k}}^\dagger)}{g} - T \text{Tr} \log[1 + e^{-H_{\text{BdG}}(\mathbf{k}, \mathbf{q}, \Delta)/T}], \quad (6)$$

where $\int_{\mathbf{k}} \equiv \int \frac{d^D k}{(2\pi)^D}$, D is the spatial dimension of the system, $\text{tr}(\dots)$ runs over spin and orbitals while $\text{Tr}[\dots]$ runs over spin, orbital and Nambu degrees of freedom. Clearly, $f(\mathbf{q}, \Delta)$ only depends on the energy eigenvalues of $H_{\text{BdG}}(\mathbf{k}, \mathbf{q})$ and is unaffected under the change $\mathbf{k} \rightarrow -\mathbf{k}$ of the integration variable. Moreover, $U(1)$ gauge symmetry mandates $f(\mathbf{q}, \Delta)$ to be unchanged under the transformation $\Delta_{\mathbf{k}} \rightarrow e^{i\phi_{\mathbf{k}}} \Delta_{\mathbf{k}}$ for arbitrary $\phi_{\mathbf{k}}$. Thus, if $\Delta_{\mathbf{k}}$ equals $\Delta_{-\mathbf{k}}$ up to a phase when the normal state possesses the symmetry \mathcal{Q} ($\mathcal{Q}\mathbb{K}$), $f(\mathbf{q}, \Delta)$ is even in \mathbf{q} : $f(\mathbf{q}, \Delta) = f(-\mathbf{q}, \Delta)$. The above condition on $\Delta_{\mathbf{k}}$ is clearly obeyed by ordinary spin singlet s -wave pairing, $\Delta_{\mathbf{k}} = \Delta \sigma_y$ with σ_y a spin Pauli matrix. Henceforth, we take pairing to be of this form and assume $\Delta_{\mathbf{k}} \equiv \Delta$ independent of \mathbf{k} . Note, Δ can still pair electrons with nonzero center-of-mass momentum $\mathbf{q}/2$.

The SDE can be calculated by minimizing $f(\mathbf{q}, \Delta)$ with respect to Δ for fixed \mathbf{q} to obtain the condensation energy $f(\mathbf{q}, \Delta) \equiv f(\mathbf{q})$ at that \mathbf{q} , followed by extremizing the supercurrent $j(\mathbf{q}) \equiv 2\partial_{\mathbf{q}} f(\mathbf{q})$ over \mathbf{q} . Positive and negative currents of largest magnitudes represent critical currents in opposite directions, j_c^\pm , and the SDE is characterized by the quality factor

$$\eta = \left| \frac{j_c^+ + j_c^-}{j_c^+ - j_c^-} \right| \in [0, 1]. \quad (7)$$

If $f(\mathbf{q}) = f(-\mathbf{q})$, critical currents in opposite directions have the same magnitude and the SDE is absent ($\eta = 0$) while the largest SDE occurs if either j_c^+ or j_c^- vanishes.

Point nodes in band structures enjoy at least one of chiral or particle-hole symmetries at low energies when the chemical potential is tuned to the node. For instance, in the absence of tilting, massless two-dimensional (2D) Dirac nodes enjoy the chiral symmetry \mathcal{Q} , three-dimensional (3D) Weyl nodes respect $\mathcal{Q}\mathbb{K}$, and 3D Dirac nodes possess both \mathcal{Q} and $\mathcal{Q}\mathbb{K}$. Crucially, while \mathcal{Q} is immediately violated by a tilt in the dispersion, $\mathcal{Q}\mathbb{K}$ survives. Therefore, to obtain a SDE with s -wave, singlet pairing in tilted Weyl and Dirac semimetals, the chemical potential must be tuned away from the node to break the particle-hole symmetry $\mathcal{Q}\mathbb{K}$ in the normal state.

Note that a finite chemical potential is not merely a density of states requirement for superconductivity to occur in the first place. Indeed, type-II semimetals already possess finite Fermi surfaces and hence, a superconducting instability with appropriate interactions. Instead, a finite chemical potential is

symmetry requirement for the SDE that goes beyond the usual mandates of broken \mathcal{T} , \mathcal{I} , and other spatial symmetries that reverse the supercurrent.

III. SDE IN A MINIMAL 1D MODEL WITH ASYMMETRIC BANDS

In this section, we focus on a 1D model with asymmetric bands. This will yield insight that will be useful for understanding the SDE for 3D Weyl and Dirac fermions. In particular, we will gradually develop the following intuition: when multiple pairing channels are present, it is possible for critical currents in opposite directions to be dominated by different channels and can, therefore, be vastly different, resulting in a large SDE.

A minimal model can be described by

$$H_{1D}(k) = (1 + \alpha k^2)k\sigma_z - \lambda k - \mu, \quad (8)$$

where μ is the chemical potential and σ_z is the Pauli-Z matrix in spin space. The parameter λ creates a tilt in the dispersion around $k = 0$ while $\alpha > 0$ ensures that the tilt is undone at finite k . H_{1D} has two qualitatively different regimes separated by a critical value of λ ,

$$\lambda_c = \left| 1 + 3 \left(\frac{\mu^2 |\alpha|}{4} \right)^{1/3} \right| \quad (9)$$

for given α and μ . For $|\lambda| < \lambda_c$, there are only two Fermi points and one momentum channel for Cooper pairing, while $|\lambda| > \lambda_c$ results in four Fermi points and three channels as sketched in Figs. 3(a) and 3(d).

For singlet superconductivity with Cooper pair momentum q , the appropriate BdG Hamiltonian is

$$H_{1D}^{\text{BdG}}(k, q) = \begin{pmatrix} H_{1D}(k + q/2) & -i\sigma_y \Delta \\ i\sigma_y \Delta & -H_{1D}^*(-k + q/2) \end{pmatrix}, \quad (10)$$

At $\mu = 0$, H_{1D} satisfies a particle-hole symmetry, $\sigma_y H_{1D}^*(k) \sigma_y = -H_{1D}(-k)$, which suppresses the SDE as described in Sec. II with $\mathcal{Q} \equiv \sigma_y$. At nonzero μ , we calculate the diode coefficient η in three different ways with increasing amount of analytical input and physical insight.

First, we directly compute the free energy density

$$f(q, \Delta) = \frac{|\Delta|^2}{g} - T \int \frac{dk}{2\pi} \text{Tr} \log \left(1 + e^{-\frac{H_{1D}^{\text{BdG}}(k, q)}{T}} \right), \quad (11)$$

minimize it with respect to Δ to obtain $\Delta(q)$ up to a phase and $f(q) \equiv f[q, \Delta(q)]$, and compute the current $j(q) = 2\partial_q f(q)$. All steps are carried out numerically and the results are shown in Fig. 1. For weak tilting, $|\lambda| < \lambda_c$, we see a single minimum in $f(q)$ close to $q = 0$ and a small diode coefficient $\eta \approx 3.2\%$ [Figs. 1(a) and 1(b)]. Strong tilting unsurprisingly produces a larger $\eta \approx 12\%$. However, the enhancement is not merely quantitative; we observe qualitatively new features in $f(q)$ in the form of two inequivalent local minima away from $q = 0$ and a large corresponding asymmetry in $j(q)$ [Figs. 1(c) and 1(d)], suggesting that the change in Fermiology plays an important role in enhancing the SDE.

To analyze this point further, we focus on T close to the critical temperature T_c where Δ is small and $f(q, \Delta)$ can be

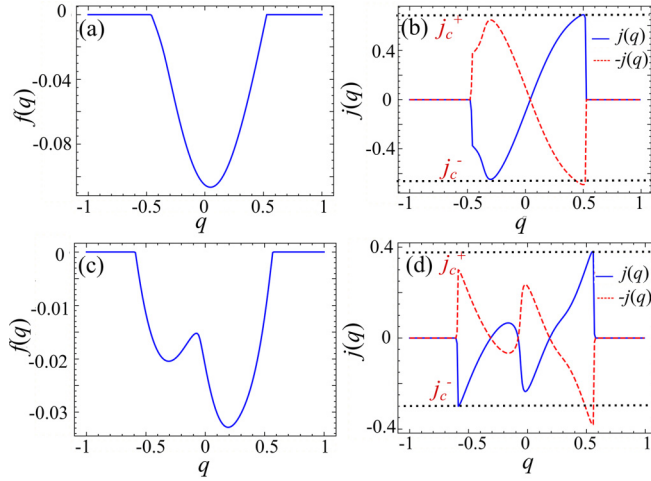


FIG. 1. (a, b) Free energy density and supercurrent with parameter $\lambda = 2$. (c, d) Free energy density and supercurrent with parameter $\lambda = 4.4$. Other parameters are $\alpha = 16$, $\mu = 0.4$, and $g = 3\pi$, which yield $\lambda_c \approx 3.58$ and $T_c \approx 0.46$, and we set $T = 0.1$.

approximated as

$$f(q, \Delta) = A(q)\Delta^2 + \frac{B(q)}{2}\Delta^4. \quad (12)$$

In this regime, the main role of $B(q)$ is to ensure physical stability by lower bounding $f(q, \Delta)$, allowing us to safely take it to be a positive constant, $B(q) \approx b > 0$ (we set $b = 1$ throughout this work). In contrast, the physics of the system depends sensitively on $A(q)$. For instance, minimizing $f(q, \Delta)$ yields a superconducting ground state with $|\Delta(q)| = \sqrt{-A(q)/b}$ only if $A(q) < 0$, while the supercurrent can be expressed as $j(q) = 2\frac{\partial}{\partial q}f(q) = |A(q)|\frac{\partial}{\partial q}A(q)$. Thus, we explicitly calculate $A(q)$ following [64] as

$$A(q) = -T \int \frac{dk}{2\pi} \sum_n \text{tr}[G(k+q, \epsilon_n)G(-k, -\epsilon_n)] + T_c \int \frac{dk}{2\pi} \sum_n \text{tr}[G(k, \epsilon_n)G(-k, -\epsilon_n)]_{T=T_c}, \quad (13)$$

where the Matsubara Green's function $G(k, \epsilon_n) = [i\epsilon_n - H_{1D}(k)]^{-1}$ with $\epsilon_n = (2n+1)\pi T$. The second term in Eq. (13) reduces to just $1/g$, which determines the value of the critical temperature T_c . The momentum integral is carried out numerically and $A(q)$ hence obtained is used to reevaluate $f(q)$ using Eq. (12). The results, shown in Fig. 2, are qualitatively consistent with the fully numerical results presented earlier. In particular, we see that $f(q)$ exhibits a single minimum, resulting in a diode quality factor of $\eta \approx 18\%$ in the weak tilting regime with $\lambda = 2$, which is less than $\lambda_c \approx 3.58$ [Figs. 2(a) and 2(b)]. In contrast, a strong tilt of $\lambda = 4.4 > \lambda_c$ shows two local minima in $f(q)$ and yields $\eta \approx 21\%$ [Figs. 2(c) and 2(d)]. Clearly, the change in Fermiology is correlated with an enhancement of the SDE. The quantitative values are different because we set $T = 0.1$, which is quite far from T_c , for numerical stability.

To unearth the connection between Fermiology and the SDE more precisely, we analytically calculate $A(q)$ in Eq. (13) in the weak pairing limit, valid for T near T_c . In this limit,

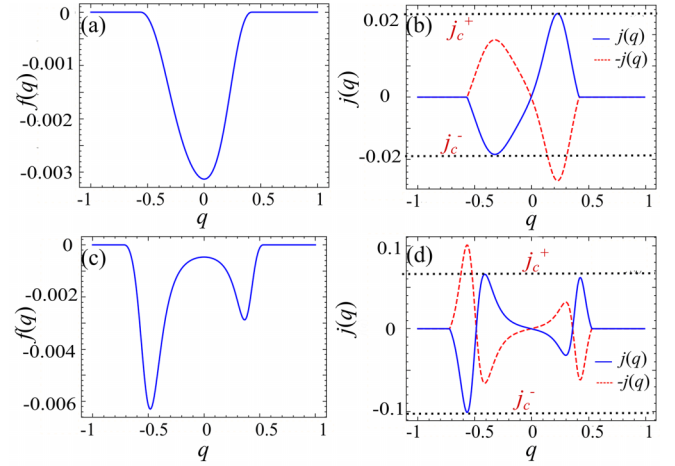


FIG. 2. (a, b) The GL free energy density $f(q)$ and the supercurrent $j(q)$ (blue line) and $-j(q)$ (red line) under weak tilting with $\lambda = 2$, respectively. (c, d) The same quantities as (a, b) under strong tilting with $\lambda = 4.4$, respectively. The parameters are $\alpha = 16$, $T_c \approx 0.46$, $T = 0.1$, and $\mu = 0.4$.

Cooper pairs predominantly form from electrons near the Fermi points. This allows us to analytically perform the Matsubara summation and momentum integral to obtain the following expression:

$$A(q) = - \sum_{i=1,2} \rho_F^{(i)} \left[\frac{T_c - T}{T_c} - \frac{7\zeta(3)}{16\pi^2 T_c^2} \delta_i^2(q) \right], \quad (14)$$

where $\delta_i(q) = (-1)^i \alpha q^3 + (-1)^{i+1} 3p_F^{(i)} \alpha q^2 - [\lambda + (-1)^{i+1} + (-1)^{i+1} 3(p_F^{(i)})^2 \alpha] q + 2\lambda p_F^{(i)}$, and $\rho_F^{(i)}$ is the density of states at the i th Fermi point. For values of $|\lambda| < \lambda_c$, the densities of states are given by

$$\rho_F^{(1)} = [2\pi(3\alpha[p_F^{(1)}]^2 + (1-\lambda))]^{-1}, \quad \rho_F^{(2)} = [2\pi(3\alpha[p_F^{(2)}]^2 + (1+\lambda))]^{-1}, \quad (15)$$

where the Fermi momentum $p_F^{(1,2)}$ are

$$p_F^{(1)} = \left[\frac{\mu}{2\alpha} + \sqrt{\frac{\mu^2}{4\alpha^2} + \frac{(1-\lambda)^3}{27\alpha^3}} \right]^{1/3} + \left[\frac{\mu}{2\alpha} - \sqrt{\frac{\mu^2}{4\alpha^2} + \frac{(1-\lambda)^3}{27\alpha^3}} \right]^{1/3}, \quad p_F^{(2)} = \left[-\frac{\mu}{2\alpha} + \sqrt{\frac{\mu^2}{4\alpha^2} + \frac{(1+\lambda)^3}{27\alpha^3}} \right]^{1/3} + \left[-\frac{\mu}{2\alpha} - \sqrt{\frac{\mu^2}{4\alpha^2} + \frac{(1+\lambda)^3}{27\alpha^3}} \right]^{1/3}. \quad (16)$$

If $p_F^{(1)} + p_F^{(2)} \neq 0$, electrons at two Fermi points can form Cooper pairs with a finite momentum $q_* \approx p_F^{(1)} + p_F^{(2)}$, where the supercurrent $j(q_*) = 0$. However, for $|\lambda| > \lambda_c$, there exist three possible Fermi momenta near $p_{F,j=1,2,3}^{(2)}$, each corresponding to a density of states $\rho_{F,j=1,2,3}^{(2)}$ for spin-up states. As illustrated in Fig. 3(b), this leads to three potential pairing

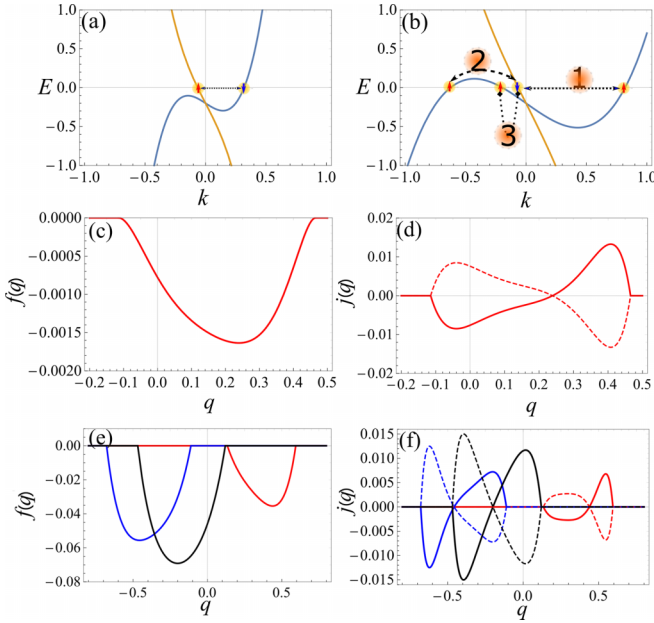


FIG. 3. (a, b) Schematics of Cooper pairs in the quasi-one-dimensional system. (c, d) The GL free energy density $f(q)$, the supercurrent $j(q)$ (solid line), and $-j(q)$ (dashed line) for weak tilting with $\lambda = 2$. The parameters are $\alpha = 16$, $\lambda = 1$, $T_c \approx 0.46$, $T = 0.1$, and $\mu = 0.4$. (e) The GL free energy density $f(q)$ for different Cooper pairs: red line (Cooper pairing channel 1), blue line (Cooper pairing channel 2), and black line (Cooper pairing channel 3). The supercurrent $j(q)$ for different Cooper pairs: red line (Cooper pairing channel 1), blue line (Cooper pairing channel 2), and black line (Cooper pairing channel 3). Dashed lines represent the opposite supercurrent $-j(q)$ for Cooper pairing channels with the same color. The parameters in (e) and (f) are the same as in (c) and (d), except that the parameter $\lambda = 4.4$.

channels with electrons having Fermi momentum near $p_F^{(1)}$ and spin-down, which leads to additional structure in the free energy density.

In general, the quality factor of the SDE depends on the model's parameters. In our 1D model, two relevant parameters are λ and μ . To elucidate the relationship between the quality factor and (μ, λ) , we present the phase diagram shown in Fig. 4(a). Interestingly, higher quality factors are observed just above the critical line [the dashed line in Fig. 4(a)], as the free energy density becomes more asymmetric in that region, as shown in Fig. 4(b). In the Bardeen-Cooper-Schrieffer (BCS) limit, an infinitesimally small attraction mediated by phonons can induce Cooper pair condensation, leading to a minimum in the free energy. Consequently, once λ reaches λ_c , a second pairing channel is established, resulting in a new minimum and inducing the largest asymmetric free energy. The transition from “one minimum” to “two minimums” is expected to occur at λ_c and give the maximum quality factor. However, our numerics cannot access this limit, hence we observe the transition just above the critical line.

We also observe that the quality factor tends to zero as λ increases. Qualitatively, for very large λ , two Fermi points that form channel 3 in Fig. 3(b) merge into a single Fermi point [see the inset band dispersions in Fig. 4(b)]. Effectively, there

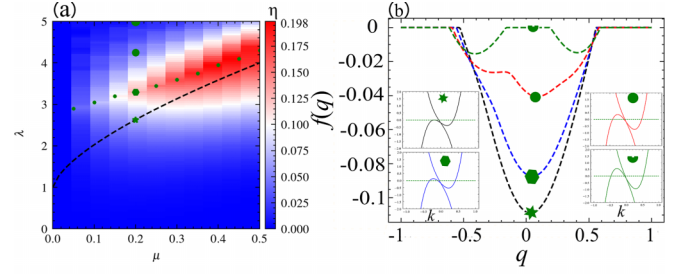


FIG. 4. (a) The quality factor $\eta(\mu, \lambda)$ for the tilted 1D model in the λ - μ plane. The dashed line represents the critical tilting value λ_c as a function of the chemical potential μ , where $\lambda_c = |1 + 3(\frac{\mu^2|\alpha|}{4})^{1/3}|$ with $\alpha = 16$. The green points depict the maximum quality factor calculated numerically. (b) The free energy density with parameters corresponding to the star, hexagon, disk, and half-disk in (a). Insets display the associated band dispersion.

are only two possible Cooper pairing channels; therefore, the diode quality factor could be diminished.

Quantitatively, we selected four typical parameters in the parameter space (denoted by the star, hexagon, disk, and half-disk), as shown in Figs. 4(a) and 4(b). At larger values of λ , the free energy density exhibits two valleys, and the two valleys are approximately mirror images of each other about the axis at $q \approx 0$. The supercurrent is defined as the derivative of the free energy density with respect to the Cooper pairing momentum. Therefore, for any positive current, there exists a negative current with the same absolute value. In other words, the diode quality factor equals zero.

Our findings not only confirm the presence of SDEs in our 1D model with asymmetric band dispersions but also underscore the significance of accounting for multiple Cooper pairing channels under strong tilting conditions. The observed complex patterns in the free energy density and supercurrent open up new avenues for optimizing superconducting systems for nonreciprocal effects.

IV. SDE IN TILTED WEYL SEMIMETALS

Weyl semimetals are materials defined by nondegenerate points of contact known as Weyl nodes, located between valence and conduction bands. These nodes exhibit linear dispersion, resulting in a variety of intriguing properties tied to the topological characteristics of the bulk band structure [57–59]. There are two principal types of Weyl semimetals: type-I, featuring point-like Fermi surfaces, and type-II, characterized by electron and hole pockets merging at the Weyl nodes [61–63]. The latter type can be derived from the former by strongly tilting the band dispersion.

In general, to realize SDEs, both \mathcal{T} - and \mathcal{I} - symmetries must be broken. The low density of states in Weyl semimetals makes breaking the \mathcal{T} - and \mathcal{I} - symmetries easier. On the other hand, as shown in the last section, we find that asymmetric band dispersions can induce the SDEs. Therefore, tilted Weyl semimetals provide us with a typical example for investigating the possibility of realizing SDEs. In this section, we introduce two simple lattice models of tilted Weyl semimetals to investigate the SDEs. The Bloch Hamiltonian describing the first

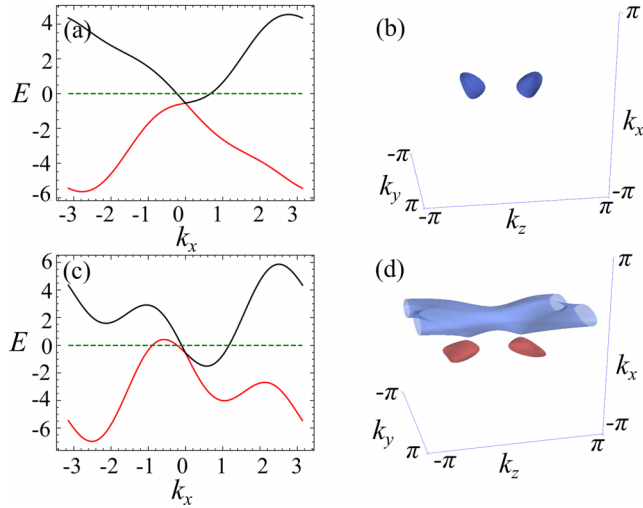


FIG. 5. (a) Projected band structure of a tilted Weyl semimetal near the Weyl node with Bloch momentum $\mathbf{k} = (0, 0, \pi/3)$. (b) Fermi surface of a weakly tilted Weyl semimetal. Parameters: $\lambda = -1/2$, $T = 0$, $g = 12$, and $\mu = 0.55$. (c, d) show the same quantities as (a, b), respectively, with the parameter $\lambda = -2$. The band dispersion remains consistent at the other Weyl node with $\mathbf{k} = (0, 0, -\pi/3)$. The red and blue Fermi surfaces in (d) are determined by E_W^- and E_W^+ in Eq. (18).

tilted Weyl semimetal and its corresponding energy spectrum can be expressed as follows:

$$H_W(\mathbf{k}) = (3 + 2 \cos k_z - 2 \cos k_x - 2 \cos k_y) \sigma_z + 2 \sin k_+ \sigma_x + 2 \sin k_- \sigma_y + (\lambda \sin 2k_x - \mu) \sigma_0, \quad (17)$$

$$E_W^\pm(\mathbf{k}) = \pm [(3 + 2 \cos k_z - 2 \cos k_x - 2 \cos k_y)^2 + 4 \sin^2 k_+ + 4 \sin^2 k_-]^{1/2} + \lambda \sin 2k_x - \mu, \quad (18)$$

where the parameter λ controls the tilt strength, $\mathbf{k} = (k_x, k_y, k_z)$ represents the Bloch momentum, μ is the chemical potential, $k_\pm = (k_x \pm k_y)/2$, and the Pauli matrices $(\sigma_x, \sigma_y, \sigma_z)$ denote spin. This model has two Weyl nodes at $\mathbf{k} = (0, 0, \pm\pi/3)$. In Figs. 5(a) and 5(c), we provide the eigenenergies as a function of k_x at $k_z = \pi/3$, $k_y = 0$ for the tilted Weyl semimetal with different tilt strengths. At $\lambda = 0$, the system Hamiltonian preserves $\mathcal{T} = \sigma_z$ but breaks $\mathcal{T} = i\sigma_y \mathbb{K}$. For nonzero λ , \mathcal{T} -symmetry is also broken while $|\lambda| > \lambda_c \approx 0.7$ renders the Weyl nodes type-II. For arbitrary λ but $\mu = 0$, $H_W(\mathbf{k})$ obeys $\sigma_x H_W^*(-\mathbf{k}) \sigma_x = -H_W(\mathbf{k})$, which is particle-hole symmetry of the form (4). Thus, $\mu \neq 0$ is necessary for a nonzero SDE.

In the presence of s -wave pairing with a nonzero Cooper pair momentum, the BdG Hamiltonian is given by

$$H_W^{\text{BdG}}(\mathbf{k}, \mathbf{q}) = \begin{pmatrix} H_W(\mathbf{k} + \mathbf{q}/2) & -i\Delta\sigma_y \\ i\Delta\sigma_y & -H_W^*(-\mathbf{k} + \mathbf{q}/2) \end{pmatrix}. \quad (19)$$

The tilt is along k_z , allowing us to set $\mathbf{q} = (0, 0, q)$. $H_W^{\text{BdG}}(\mathbf{k}, q)$ satisfies the particle-hole symmetry $\tau_x \mathbb{K} H_W^{\text{BdG}}(\mathbf{k}, q) \mathbb{K} \tau_x = -H_W^{\text{BdG}}(-\mathbf{k}, q)$, which ensures the existence of pairs of opposite eigenvalues $E_\pm(-\mathbf{k})$ and $-E_\pm(\mathbf{k})$.

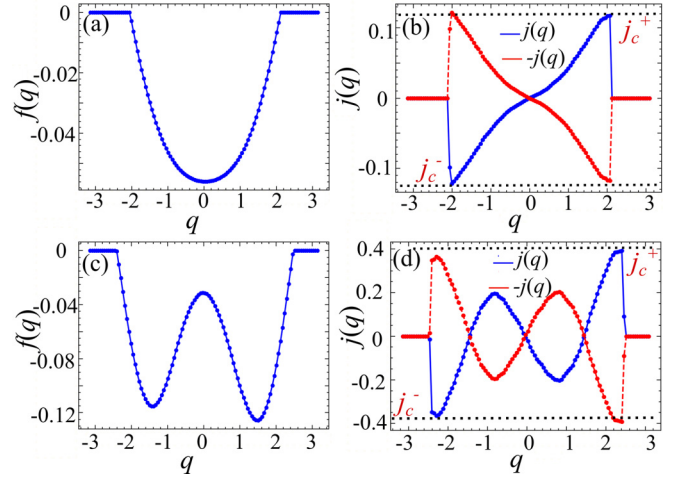


FIG. 6. (a, b) The free energy density $f(q)$, the supercurrent $j(q)$ (blue dotted line), and $-j(q)$ (red dotted line) for $\lambda = -1/2$, $T = 0$, $g = 12$, and $\mu = 0.55$. (c, d) The same quantities as (a, b) with the parameter $\lambda = -2$.

In the 1D model, we observe that the strong tilting gives rise to more pairing channels, which create new structures in the free energy density and the supercurrent and enhance the SDE. In the 3D model, the number and details of the pairing channels will depend on the transverse momenta (k_x, k_y) in general. The 3D model with band tilting along the k_z -direction could be thought of as a 1D model with tilted band dispersion labeled by the parameters (k_x, k_y) , and the tilting strength depends on the values of the parameters (k_x, k_y) . Therefore, a similar enhancement as in the 1D model is expected to occur in the 3D model. To investigate this possibility, we numerically calculate $f(q)$ and $j_z(q) \equiv j(q)$ at $T = 0$. As shown in Fig. 5(a), for a relatively small tilt for a given μ , there is only one type of pairing channel, only one minimum in $f(q)$, and a small difference between j_c^\pm that yield a diode quality factor of $\eta \approx 1.8\%$. However, for a larger tilted strength, three different types of Cooper pairing channels are present, which induce two minima in $f(q)$ a larger difference between j_c^+ and j_c^- are boosted diode quality factor of $\eta \approx 3.7\%$ [see Figs. 6(c) and 6(d)].

We perform a similar analysis on a different lattice model of a tilted Weyl semimetal. In addition to the pockets near the Weyl nodes for the chosen parameters, there are Fermi pockets near the Brillouin zone boundary. Therefore, this model could support more possible Cooper pairing channels, and the SDE could be enhanced. The Bloch Hamiltonian describing the tilted Weyl semimetal and its corresponding energy spectrum can be expressed as

$$\tilde{H}_W(\mathbf{k}) = 2(\cos k_x - \cos k_0 - \cos k_y - \cos k_z + 2) \sigma_x + 2 \sin k_y \sigma_y + 2 \sin k_z \sigma_z + (\lambda \sin 2k_z - \mu) \sigma_0, \quad (20)$$

$$\tilde{E}_W^\pm(\mathbf{k}) = \pm 2[(\cos k_x - \cos k_0 - \cos k_y - \cos k_z + 2)^2 + \sin^2 k_y + \sin^2 k_z]^{1/2} + \lambda \sin 2k_z - \mu. \quad (21)$$

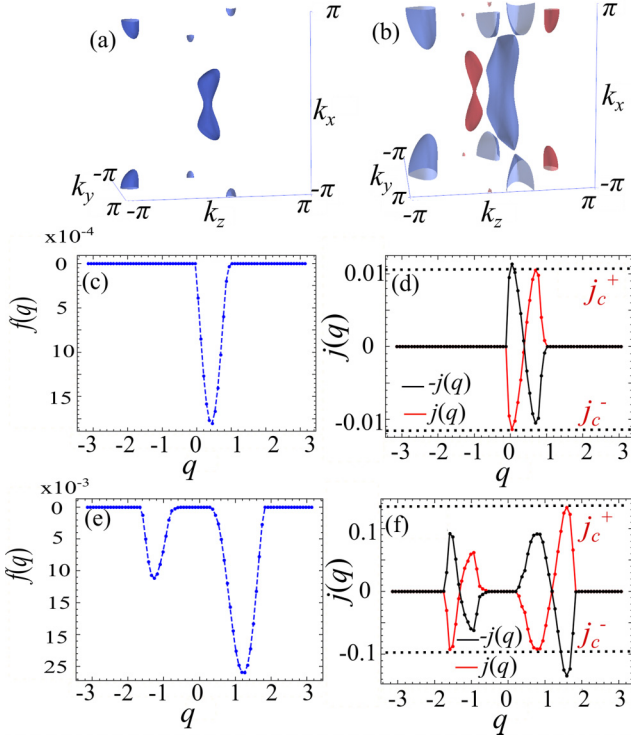


FIG. 7. (a, b) Fermi pockets of the tilted Weyl semimetal. (c, d) The free energy density $f(q)$, the supercurrent $j(q)$ (red dotted line), and $-j(q)$ (black dotted line) for $\lambda = -1$, $T = 0$, $g = 10$, and $\mu = 0.4$. (e, f) The same quantities as (c, d) with the parameter $\lambda = -2$.

This model has two Weyl nodes at $\mathbf{k} = (\pm k_0, 0, 0)$; we set $k_0 = \pi/4$ henceforth. In Figs. 7(a) and 7(b), we show the Fermi pockets for the tilted Weyl semimetal with different tilt strengths. At $\lambda = 0$, the system Hamiltonian preserves $\mathcal{I} = \sigma_x$ but breaks \mathcal{T} -symmetry. For nonzero λ , \mathcal{I} is also broken while $|\lambda| > 1$ renders the type-II Weyl nodes. For arbitrary λ but $\mu = 0$, $\tilde{H}_W(\mathbf{k})$ obeys $\sigma_z \tilde{H}_W^*(-\mathbf{k}) \sigma_z = -\tilde{H}_W(\mathbf{k})$, which is particle-hole symmetry of the form Eq. (4).

In the presence of s -wave pairing with a nonzero Cooper pair momentum, the BdG Hamiltonian is given by

$$\tilde{H}_W^{\text{BdG}}(\mathbf{k}, \mathbf{q}) = \begin{pmatrix} \tilde{H}_W(\mathbf{k} + \mathbf{q}/2) & -i\Delta\sigma_y \\ i\Delta\sigma_y & -\tilde{H}_W^*(-\mathbf{k} + \mathbf{q}/2) \end{pmatrix}. \quad (22)$$

The tilt is along k_z , allowing us to set $\mathbf{q} = (0, 0, q)$. $\tilde{H}_W^{\text{BdG}}(\mathbf{k}, q)$ satisfies the particle-hole symmetry $\tau_x \mathbb{K} \tilde{H}_W^{\text{BdG}}(\mathbf{k}, q) \mathbb{K} \tau_x = -\tilde{H}_W^{\text{BdG}}(-\mathbf{k}, q)$, which ensures the existence of pairs of opposite eigenvalues $\tilde{E}_\pm(-\mathbf{k})$ and $-\tilde{E}_\pm(\mathbf{k})$.

As shown in Figs. 7(c) and 7(d), for a relatively small tilt for a given μ , there is only one minimum in $f(q)$ and a small difference between j_c^\pm that yield a diode quality factor of $\eta \approx 3.8\%$. However, for a larger tilted strength, two minima in $f(q)$ a larger difference between j_c^+ and j_c^- are the boosted diode quality factor of $\eta \approx 18.4\%$ [see Figs. 7(e) and 7(f)]. The quality factor of the SDE in this model is much higher than the diode quality factor in the first model, confirming that multiple Cooper pairing channels can enhance the diode quality factor.

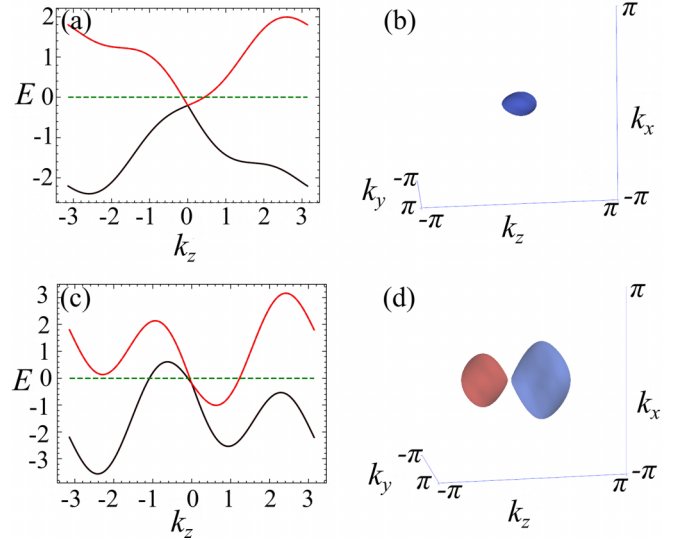


FIG. 8. (a) Projected band structure of the Dirac semimetal. (b) Fermi surface for $\lambda = -0.3$, $T = 0$, $g = 2.6$, and $\mu = 0.2$. (c, d) Same quantities as in (a, b), with the parameters being identical to those in (a, b), except for the parameter $\lambda = -1.5$. The red and blue Fermi surfaces in (d) are determined by \tilde{E}_W^- and \tilde{E}_W^+ in Eq. (21).

V. SDE IN TILTED DIRAC SEMIMETALS

Similar to Weyl semimetals, in a Dirac semimetal, the valence and conduction bands touch linearly at specific points in the Brillouin zone, known as Dirac points, where the energy dispersion relation is linear in momentum [54–56]. The existence of these 3D Dirac points is of profound significance in condensed matter physics. At the quantum critical point, where a transition occurs between a normal insulator and a topological insulator, a three-dimensional Dirac semimetal manifests [65]. This quantum critical point represents a delicate balance between different electronic states, resulting in the appearance of a Dirac semimetal phase that possesses distinct topological properties. The formation of this exotic phase further highlights the role of symmetries in dictating the behavior of electronic states and their topological nature.

In the last section, we showed that SDE could be realized in tilted Weyl semimetals. Due to the similarity between Weyl semimetals and Dirac semimetals, a natural question arises: Can introducing a perturbation term to the Dirac semimetal, which tilts the band dispersion and breaks both \mathcal{T} - and \mathcal{I} -symmetries, support the emergence of SDEs? To answer this question, we consider a lattice model of the Dirac semimetals and study the possibility of SDEs induced by the tilting.

We focus on a cubic lattice model with a single Dirac point at the $\Gamma = (0, 0, 0)$ point. The dispersion is tilted in a specific direction, assumed to be in the z -direction as shown in Fig. 8. The Bloch Hamiltonian is

$$\begin{aligned} H_D(\mathbf{k}) = & \sin k_x \Gamma_{zy} + \sin k_y \Gamma_{zx} + \sin k_z \Gamma_{y0} \\ & + (3 - \cos k_x - \cos k_y - \cos k_z) \Gamma_{x0} \\ & + (\lambda \sin k_z - \mu) \Gamma_{00}, \end{aligned} \quad (23)$$

where the matrix $\Gamma_{ab} \equiv \tau_a \otimes \sigma_b$ with $a, b \in (0, x, y, z)$. The term proportional to λ induces tilting and breaks the \mathcal{T} - and \mathcal{I} -

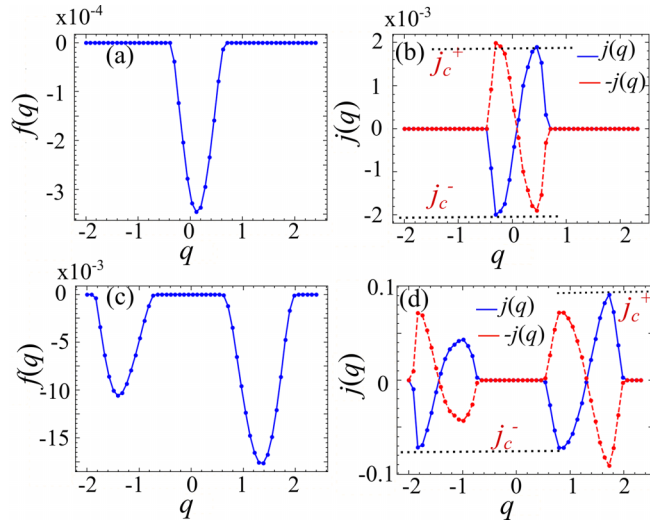


FIG. 9. (a, b) Free energy density $f(q)$, supercurrent $j(q)$ (blue dotted line), and $-j(q)$ (red dotted line) for parameters $\lambda = -0.3$, $T = 0$, $g = 2.6$, and $\mu = 0.2$. (c, d) Same quantities as in (a, b) with identical parameters, except for $\lambda = -1.5$.

symmetries while a nonzero μ is needed to break symmetries studied in Sec. II.

s -wave superconductivity is captured by the BdG Hamiltonian

$$H_D^{\text{BdG}}(\mathbf{k}, \mathbf{q}) = \begin{pmatrix} H_D(\mathbf{k} + \mathbf{q}/2) & -i\Delta\sigma_y \\ i\Delta\sigma_y & -H_D^*(-\mathbf{k} + \mathbf{q}/2) \end{pmatrix}. \quad (24)$$

As demonstrated in Fig. 9, our investigation reveals intriguing similarities between the free energy density and the SDEs observed in Dirac semimetals and those previously observed in Weyl semimetals. The quality factor $\eta \approx 2.5\%$ at weak tilting with $\lambda = -0.3$ and $\eta \approx 11.7\%$ at stronger tilting with $\lambda = -1.5$. This enhancement is accompanied by the appearance of multiple pairing channels and multiple minima in the free energy. These behaviors motivate exploring tilted Dirac semimetals as well for the realization of SDEs.

VI. CANDIDATE MATERIALS

For materials with broken \mathcal{T} - and \mathcal{I} -symmetries, the realization of SDEs might be hindered by additional lattice symmetries, such as mirror symmetry or reflection symmetry.

Consequently, these additional symmetries would also need to be broken to enable the occurrence of SDEs. One such material exemplifying this is Ti_2MnAl , with space group $F\bar{4}3M$ (No. 216) [66]. In Ti_2MnAl , weak spin-orbit coupling further breaks the mirror symmetry ($M_{\pm 110}$), leading to different tilts between the two mirror-symmetric Weyl points. Another set of materials can be found in the RAIX family with the space group $I4_1md$ (No. 109), where R represents rare earth metals like Pr, Ce, and Sm, and X denotes Ge or Si [67,68]. These materials lack horizontal mirror symmetry, which increases the likelihood of asymmetric bands in the z -direction. If superconductivity could be realized in them, then they are potential candidate materials for verifying our theoretical studies.

VII. CONCLUSION

In this work, we delved into the intriguing phenomenon of SDEs in topological semimetals. We demonstrated, by investigating a simple 1D toy model using various numerical and analytical methods, that multiple pairing channels rather than tilting the dispersion enrich the superconducting physics and enhance the SDE. We carried this understanding to 3D Weyl and Dirac semimetals, showed the existence of the SDE in these systems, and demonstrated its enhancement due to multiple Fermi pockets and pairing channels.

While our toy models are too simple to fully capture the complexity of tilting topological semimetals, they do demonstrate the potential for SDEs in such systems if the necessary symmetries, such as time-reversal, inversion, and reflection symmetry, are broken. Furthermore, they indicate that the tilting strength can influence and tune the quality factor of SDEs in tilted topological semimetals. Our findings hold implications for future explorations of superconducting phenomena and topological effects in condensed matter systems. Moreover, the intrinsic nature of SDEs in the presence of asymmetric band dispersions suggests a promising avenue for designing advanced superconducting devices and harnessing nonreciprocal transport in quantum technologies. Ultimately, this research opens up new directions for investigating emergent phenomena at the intersection of superconductivity and topological physics.

ACKNOWLEDGMENTS

This work was supported by the Department of Energy Grant No. DE-SC0022264.

- [1] F. Ando, Y. Miyasaka, T. Li, J. Ishizuka, T. Arakawa, Y. Shiota, T. Moriyama, Y. Yanase, and T. Ono, *Nature (London)* **584**, 373 (2020).
- [2] J. Linder and J. W. A. Robinson, *Nat. Phys.* **11**, 307 (2015).
- [3] T. Golod and V. M. Krasnov, *Nat. Commun.* **13**, 3658 (2022).
- [4] B. Pal, A. Chakraborty, M. Sivakumar, Pranava K. and Davydova, A. K. Gopi, A. K. Pandeya, J. A. Krieger, Y. Zhang, M. Date, S. Ju, N. Yuan, L. Schröter, Niels B. M. and Fu, and S. S. P. Parkin, *Nat. Phys.* **18**, 1228 (2022).
- [5] K. Jiang and J. Hu, *Nat. Phys.* **18**, 1145 (2022).

- [6] M. Nadeem, M. S. Fuhrer, and X. Wang, [arXiv:2301.13564](https://arxiv.org/abs/2301.13564).
- [7] H. Narita, J. Ishizuka, R. Kawarazaki, D. Kan, Y. Shiota, T. Moriyama, Y. Shimakawa, A. V. Ognev, A. S. Samardak, Y. Yanase, and T. Ono, *Nat. Nanotechnol.* **17**, 823 (2022).
- [8] J.-X. Lin, P. Siriviboon, H. D. Scammell, S. Liu, D. Rhodes, K. Watanabe, T. Taniguchi, J. Hone, M. S. Scheurer, and J. I. A. Li, *Nat. Phys.* **18**, 1221 (2022).
- [9] H. D. Scammell, J. I. A. Li, and M. S. Scheurer, *2D Mater.* **9**, 025027 (2022).

- [10] J. Díez-Mérida, A. Díez-Carlón, S. Y. Yang, Y.-M. Xie, X.-J. Gao, J. Senior, K. Watanabe, T. Taniguchi, X. Lu, A. P. Higginbotham, K. T. Law, and D. K. Efetov, *Nat. Commun.* **14**, 2396 (2023).
- [11] L. Bauriedl, C. Bäuml, L. Fuchs, C. Baumgartner, N. Paulik, J. M. Bauer, K.-Q. Lin, J. M. Lupton, T. Taniguchi, K. Watanabe, C. Strunk, and N. Paradiso, *Nat. Commun.* **13**, 4266 (2022).
- [12] C. Baumgartner, L. Fuchs, A. Costa, S. Reinhardt, S. Gronin, G. C. Gardner, T. Lindemann, M. J. Manfra, P. E. Faria Junior, D. Kochan, J. Fabian, N. Paradiso, and C. Strunk, *Nat. Nanotechnol.* **17**, 39 (2022).
- [13] H. Wu, Y. Wang, Y. Xu, C. Sivakumar, Pranava K. and Pasco, U. Filippozzi, S. S. P. Parkin, Y.-J. Zeng, T. McQueen, and M. N. Ali, *Nature (London)* **604**, 653 (2022).
- [14] M. Gupta, G. V. Graziano, M. Pendharkar, J. T. Dong, C. P. Dempsey, C. Palmstrøm, and V. S. Pribiag, *Nat. Commun.* **14**, 3078 (2023).
- [15] M. Trahms, L. Melischek, J. F. Steiner, B. Mahendru, I. Tamir, N. Bogdanoff, O. Peters, G. Reecht, C. B. Winkelmann, F. von Oppen, and K. J. Franke, *Nature (London)* **615**, 628 (2023).
- [16] Y. Hou, F. Nichele, H. Chi, A. Lodesani, Y. Wu, M. F. Ritter, D. Z. Haxell, M. Davydova, S. Ilić, O. Glezakou-Elbert, A. Varambally, F. S. Bergeret, A. Kamra, L. Fu, P. A. Lee, and J. S. Moodera, *Phys. Rev. Lett.* **131**, 027001 (2023).
- [17] A. Gutfreund, H. Matsuki, V. Plastovets, A. Noah, L. Gorzawski, N. Fridman, G. Yang, A. Buzdin, O. Millo, J. W. A. Robinson, and Y. Anahory, *Nat. Commun.* **14**, 1630 (2023).
- [18] K. Yasuda, H. Yasuda, T. Liang, R. Yoshimi, A. Tsukazaki, K. S. Takahashi, N. Nagaosa, M. Kawasaki, and Y. Tokura, *Nat. Commun.* **10**, 2734 (2019).
- [19] M. Masuko, M. Kawamura, R. Yoshimi, M. Hirayama, Y. Ikeda, R. Watanabe, J. J. He, D. Maryenko, A. Tsukazaki, K. S. Takahashi, M. Kawasaki, N. Nagaosa, and Y. Tokura, *npj Quantum Mater.* **7**, 104 (2022).
- [20] T. Karabassov, I. V. Bobkova, A. A. Golubov, and A. S. Vasenko, *Phys. Rev. B* **106**, 224509 (2022).
- [21] K. Ishihara, L. D. Anh, T. Hotta, K. Inagaki, M. Kobayashi, and M. Tanaka, *arXiv:2308.00893*.
- [22] N. F. Q. Yuan and L. Fu, *Proc. Natl. Acad. Sci. USA* **119**, e2119548119 (2022).
- [23] A. Daido, Y. Ikeda, and Y. Yanase, *Phys. Rev. Lett.* **128**, 037001 (2022).
- [24] P. Fulde and R. A. Ferrell, *Phys. Rev.* **135**, A550 (1964).
- [25] A. Larkin and Y. N. Ovchinnikov, *Sov. Phys. JETP* **20**, 762 (1965).
- [26] A. Daido and Y. Yanase, *Phys. Rev. B* **106**, 205206 (2022).
- [27] H. F. Legg, D. Loss, and J. Klinovaja, *Phys. Rev. B* **106**, 104501 (2022).
- [28] P. Hosur and D. Palacios, *Phys. Rev. B* **108**, 094513 (2023).
- [29] S. Ilić and F. S. Bergeret, *Phys. Rev. Lett.* **128**, 177001 (2022).
- [30] Y. Zhang, Y. Gu, P. Li, J. Hu, and K. Jiang, *Phys. Rev. X* **12**, 041013 (2022).
- [31] M. Davydova, S. Prembabu, and L. Fu, *Sci. Adv.* **8**, eabo0309 (2022).
- [32] R. S. Souto, M. Leijnse, and C. Schrade, *Phys. Rev. Lett.* **129**, 267702 (2022).
- [33] D. Wang, Q.-H. Wang, and C. Wu, *arXiv:2209.12646*.
- [34] X. P. Yang, Y. Zhong, S. Mardanya, T. A. Cochran, R. Chapai, A. Mine, J. Zhang, J. Sánchez-Barriga, Z.-J. Cheng, O. J. Clark *et al.*, *Phys. Rev. Lett.* **130**, 046402 (2023).
- [35] Amit and Y. Singh, *Phys. Rev. B* **97**, 054515 (2018).
- [36] P. Garcia-Campos, Y. K. Huang, A. de Visser, and K. Hasselbach, *Phys. Rev. B* **103**, 104510 (2021).
- [37] S. Das, Amit, A. Sirohi, L. Yadav, S. Gayen, Y. Singh, and G. Sheet, *Phys. Rev. B* **97**, 014523 (2018).
- [38] D. Yan, D. Geng, Q. Gao, Z. Cui, C. Yi, Y. Feng, C. Song, H. Luo, M. Yang, M. Arita *et al.*, *Phys. Rev. B* **102**, 205117 (2020).
- [39] F. Fei, X. Bo, P. Wang, J. Ying, J. Li, K. Chen, Q. Dai, B. Chen, Z. Sun, M. Zhang *et al.*, *Adv. Mater.* **30**, 1801556 (2018).
- [40] J. Luo, Y. Li, J. Li, T. Hashimoto, T. Kawakami, H. Lu, S. Jia, M. Sato, and J. Wang, *Phys. Rev. Mater.* **3**, 124201 (2019).
- [41] Y. Li, Y. Zhou, Z. Guo, F. Han, X. Chen, P. Lu, X. Wang, C. An, Y. Zhou, J. Xing *et al.*, *npj Quantum Mater.* **2**, 66 (2017).
- [42] Y. Qi, P. G. Naumov, M. N. Ali, C. R. Rajamathi, W. Schnelle, O. Barkalov, M. Hanfland, S.-C. Wu, C. Shekhar, Y. Sun *et al.*, *Nat. Commun.* **7**, 11038 (2016).
- [43] Z. Guguchia, F. von Rohr, Z. Shermadini, A. T. Lee, S. Banerjee, A. Wieteska, C. Marianetti, B. Frandsen, H. Luetkens, Z. Gong *et al.*, *Nat. Commun.* **8**, 1082 (2017).
- [44] W. Duan, J. Zhang, R. Kumar, H. Su, Y. Zhou, Z. Nie, Y. Chen, M. Smidman, C. Cao, Y. Song *et al.*, *Phys. Rev. B* **106**, 214521 (2022).
- [45] H. Wang, H. Wang, H. Liu, H. Lu, W. Yang, S. Jia, X.-J. Liu, X. Xie, J. Wei, and J. Wang, *Nat. Mater.* **15**, 38 (2016).
- [46] Y. Xing, H. Wang, C.-K. Li, X. Zhang, J. Liu, Y. Zhang, J. Luo, Z. Wang, Y. Wang, L. Ling *et al.*, *npj Quantum Mater.* **1**, 16005 (2016).
- [47] Y. Li, C. An, C. Hua, X. Chen, Y. Zhou, Y. Zhou, R. Zhang, C. Park, Z. Wang, Y. Lu *et al.*, *npj Quantum Mater.* **3**, 58 (2018).
- [48] G. Y. Cho, J. H. Bardarson, Y.-M. Lu, and J. E. Moore, *Phys. Rev. B* **86**, 214514 (2012).
- [49] L. Hao, R. Wang, P. Hosur, and C. S. Ting, *Phys. Rev. B* **96**, 094530 (2017).
- [50] H. Wei, S.-P. Chao, and V. Aji, *Phys. Rev. B* **89**, 014506 (2014).
- [51] P. Hosur, X. Dai, Z. Fang, and X.-L. Qi, *Phys. Rev. B* **90**, 045130 (2014).
- [52] M. Alidoust and K. Halterman, *Phys. Rev. B* **101**, 035120 (2020).
- [53] P. Dutta, F. Parhizgar, and A. M. Black-Schaffer, *Phys. Rev. B* **101**, 064514 (2020).
- [54] S. M. Young, S. Zaheer, J. C. Y. Teo, C. L. Kane, E. J. Mele, and A. M. Rappe, *Phys. Rev. Lett.* **108**, 140405 (2012).
- [55] S. M. Young and C. L. Kane, *Phys. Rev. Lett.* **115**, 126803 (2015).
- [56] Q. D. Gibson, L. M. Schoop, L. Muechler, L. S. Xie, M. Hirschberger, N. P. Ong, R. Car, and R. J. Cava, *Phys. Rev. B* **91**, 205128 (2015).
- [57] P. Hosur and X. Qi, *C. R. Phys.* **14**, 857 (2013).
- [58] B. Yan and C. Felser, *Annu. Rev. Condens. Matter Phys.* **8**, 337 (2017).
- [59] N. P. Armitage, E. J. Mele, and A. Vishwanath, *Rev. Mod. Phys.* **90**, 015001 (2018).
- [60] G. Bednik, A. A. Zyuzin, and A. A. Burkov, *Phys. Rev. B* **92**, 035153 (2015).
- [61] A. A. Zyuzin and R. P. Tiwari, *JETP Lett.* **103**, 717 (2016).
- [62] S. Tchoumakov, M. Civelli, and M. O. Goerbig, *Phys. Rev. Lett.* **117**, 086402 (2016).

- [63] A. A. Soluyanov, D. Gresch, Z. Wang, Q. Wu, M. Troyer, X. Dai, and B. A. Bernevig, *Nature (London)* **527**, 495 (2015).
- [64] J. J. He, Y. Tanaka, and N. Nagaosa, *New J. Phys.* **24**, 053014 (2022).
- [65] S. Murakami, *New J. Phys.* **9**, 356 (2007).
- [66] W. Shi, L. Muechler, K. Manna, Y. Zhang, K. Koepf, R. Car, J. van den Brink, C. Felser, and Y. Sun, *Phys. Rev. B* **97**, 060406(R) (2018).
- [67] D. S. Sanchez, G. Chang, I. Belopolski, H. Lu, J.-X. Yin, N. Alidoust, X. Xu, T. A. Cochran, X. Zhang, Y. Bian, S. S. Zhang, Y.-Y. Liu, J. Ma, G. Bian, H. Lin, S.-Y. Xu, S. Jia, and M. Z. Hasan, *Nat. Commun.* **11**, 3356 (2020).
- [68] G. Chang, B. Singh, S.-Y. Xu, G. Bian, S.-M. Huang, C.-H. Hsu, I. Belopolski, N. Alidoust, D. S. Sanchez, H. Zheng, H. Lu, X. Zhang, Y. Bian, T.-R. Chang, H.-T. Jeng, A. Bansil, H. Hsu, S. Jia, T. Neupert, H. Lin *et al.*, *Phys. Rev. B* **97**, 041104(R) (2018).